Volume 13, Issue 2, Page 61-68, 2024 https://doi.org/10.46810/tdfd.1412214 Research Article

BİNGÖL UNIVERSITY

Türk Doğa ve Fen Dergisi
Turkish Journal of Nature and Science
www.dergipark.gov.tr/tdfd

Refractive Index Sensor Based on Terahertz Metamaterial Absorber with High Sensitivity and Quality Factor for Sensing Applications

Ahmet TEBER[1*]

[1] Bayburt University, Department of Electrical and Energy, Bayburt, Türkiye
Ahmet TEBER ORCID No: 0000-0002-7361-2302

**Corresponding author: ahmetteber@bayburt.edu.tr*

(Received: 30.12.2023, Accepted: 24.05.2024, Online Publication: 28.06.2024)

Keywords
Absorber, Polarization-independent, Refractive-index, Sensing, Sensor

Abstract: This research describes and assesses a terahertz metamaterial absorber (TMA) with a simple and easy-to-produce structure consisting of gold-silicon (optical)-gold design as a refractive index sensing. Due to the high field limitation in the detection regime, electromagnetic (EM) wave's absorption reaches 99.40% at a frequency of 3.719 THz, including a significant quality factor (Q-Factor) of 65.77 and a figure of merit, FoM, of 21.49. The TMA has a remarkable sensitivity of 1.215 THz/RIU and can be used as a refractive index sensor (RIS). The proposed metamaterial absorber-based sensor is susceptible to refractive index changes (1.00 to 1.05) in the surrounding medium. For the physical absorption mechanism, the fundamental absorption peak is mainly due to the simultaneous occurrence of electric and magnetic dipole resonances. The proposed absorber has the feature of being an excellent RIS due to its sensing and detection applications.

Algılama Uygulamaları için Yüksek Hassasiyet ve Kalite Faktörüne Sahip Terahertz Metamalzeme Soğurucu Tabanlı Kırılma İndeks Sensörü

Anahtar Kelimeler
Soğurma, Polarizasyon-bağımsız, Kırılma-indeksi, Algılama, Sensör

Öz: Bu araştırma, kırılma indisi algılaması olarak altın-silikon (optik)-altın tasarımından oluşan basit ve üretimi kolay bir yapıya sahip terahertz metamalzeme soğurucuyu (TMA) tanımlamakta ve değerlendirmektedir. Tespit rejimindeki yüksek alan sınırlaması nedeniyle, elektromanyetik (EM) dalganın emilimi, 65,77'lik önemli bir kalite faktörü (Q-Faktörü) ve 21,49'luk bir başarı rakamı olan FoM dahil olmak üzere, 3,719 THz frekansta %99,40'a ulaşır. TMA, 1,215 THz/RIU'luk makul bir hassasiyet sergileyen bir kırılma indisi sensörü (RIS) olarak kullanılabilir. Metamalzeme soğurucu tabanlı sensör, çevredeki ortamdaki kırılma indisi değişikliklerine (1,00 ila 1,05) karşı hassastır. Soğurma mekanizması için, temel soğurma zirvesi esas olarak elektrik ve manyetik dipol rezonanslarının eşzamanlı oluşumundan kaynaklanmaktadır. Önerilen soğurucu, algılama ve tespit uygulamaları nedeniyle mükemmel bir RIS olma özelliğine sahiptir.

1. INTRODUCTION

Since materials extracted from nature rarely interact with terahertz (THz) frequencies, artificial metamaterials are critical in interacting with electromagnetic (EM) waves at THz frequencies. Thanks to their exclusive features, such as excellent absorption/transmission and stealth, metamaterials reveal an extensive range of potential uses, such as sensors [1-6], absorbers [7-9], and imaging [10-12]. It has excellent potential in chemistry and medicine, such as biomolecular sensing, metamaterial devices, and diagnostic devices for cancer and infectious diseases. Metamaterial structures attract the attention of researchers due to their new and distinctive properties, which are very difficult to obtain by natural means, their excellent performance, especially in sensing, and their broad application capabilities.

In a TMA structure, absorption performances (peaks) can be adjusted by altering certain structural parameters. Thus, TMAs can be sensors in numerous applications [13-16]. Biosensors [17-19] and temperature sensors [20,21] are designed as sensing applications. It is also clear that thickness and temperature sensing are not the only areas of use of terahertz metamaterials. In this regard, the use of TMAs in sensing the refractive index of the medium surrounding the sensor is available in the literature. In studies on detecting the refractive index (RI) of the encircling medium, quality factor (Q-factor),

a figure of merit (FoM), refractive index range under examination, and step size (refractive index unit) are important parameters. Table 1 lists some studies in the literature based on these parameters.

Table 1. A comparison of the reported absorbers and the suggested TMA's sensing parameters

Reference	Q-factor	FoM	RI's Range	Step Size (RIU)	Band Type
[1]	22.05	2.94	η=1.0-1.39	0.05	Single
[22]	32.167	6.015	η=1.1-1.90	0.20	Single
[23]	132.05	8.887	η=1.0-1.10	0.02	Multi
[24]	N/A	N/A	η=1.0-2.00	0.2	Multi
[25]	7.036	2.67	η=1.0-1.80	0.2	Single
[26]	8.5	0.85	η=1.0-2.00	0.2	Multi
[27]	5.5	0.4	η=1.0-1.40	0.1	Single
[28]	35.36	94.05	η=1.0-1.05	0.01	Single
[29]	296.3	229	η=1.0-1.10	0.02	Dual
The Proposed Study	**65.77**	**21.49**	**η=1.0-1.05**	**0.01**	**Single**

It is essential to highlight some critical studies in the literature where the refractive index changes of the encircling medium are sensitive. As of 2019, a metamaterial absorber design with a near-perfect absorption response for terahertz sensing applications was projected and analyzed with a sensitivity of 300GHz/RIU [1]. In studies on biomedical samples, the refractive index of most models is between 1.3 and 1.39, and the sensor reported in the author's study has high sensitivity for biomedical applications. An ultrathin multiband TMA was proposed in another study [23]. Simulation results reported near-perfect absorption (in the frequency range of 4.5 THz-6.0 THz). The authors also analyzed the impact of changes in the refractive index of the medium surrounding the absorber on the detection performances and implications of the analyte's thickness. They reported a sensitivity of 471 GHZ/RIU in a narrow refractive index range (η=1.0-1.1), noting that the presented absorber has potential applications in photodetectors, multispectral, biosensors, and imaging. In another study [28], a stainless-steel metamaterial absorber operating at THz was demonstrated. In this study, unlike metamaterial absorbers created with a sandwich structure (metal/dielectric/metal), they are made entirely of stainless-steel materials that do not contain a sandwich structure (metal metamaterial and substrate material). Thus, the authors reduced costs by aiming to simplify the production process. According to their results, by achieving a relatively high-quality factor (Q = 35.36) and a sensitivity of 74.18 μm/RIU based on the wavelength of resonance frequency, they presented sensor studies with a very high sensitivity compared to their counterparts. A dual-band TMA has been demonstrated by Wang et al. [29] Although the quality factor (6.9156) was too low in the first double-band absorption peak, they obtained a quality factor of approximately 296.3 in the second peak. It is also highlighted that the RIS exhibits a sensitivity of 1900GHz/RIU for the second resonance peak.

We present a simple and easy-to-fabricate terahertz metamaterial absorber with a gold-silicon (optical)-gold sandwich structure for terahertz sensing applications. Taking the studies given as a reference, we chose a smaller step size (0.01) of the refractive index of the medium surrounding the sensor. We offer an excellent RIS for sensing and detection applications with an acceptable high sensitivity compared to its counterparts, 1215GHz/RIU, and a high-quality factor (Q=65.77). The study's organization can be given as follows: first, the structural design of the proposed RIS is presented in the next section, and then the simulation results are reported in Section 3. Then, the polarization dependence of the proposed RIS is examined. A detailed discussion of the appearance of absorption peaks concerning refractive index changes is presented using the available scatter plots. A parametrical analysis is additionally performed to verify the selection of parameters, and lastly, the absorption mechanism is addressed by simulating the electric, magnetic field, and surface current distributions.

2. METHODS AND DESIGNATION

2.1. Absorption Method and Designation of Proposed Structure

The metasurface consisting of gold (Au), which has a four-armed structure and an electrical conductivity (σ) of 4.561e7 S/m, forms the upper part of the sandwich structure. The first of the arms was created as a rectangular structure with width w and length R along the y-axis. Afterward, this rectangular structure was moved away from the origin point by g. An arm of the unit cell was created by removing two identical triangular structures from the upper edges of the rectangular structure. After completing three more identical components to this arm, they were positioned on the silicon (optical) substrate material with 45-degree angle increments clockwise. The base surface of the substrate material was covered entirely with Gold (Au) to obtain a sandwich structure (Figure 1).

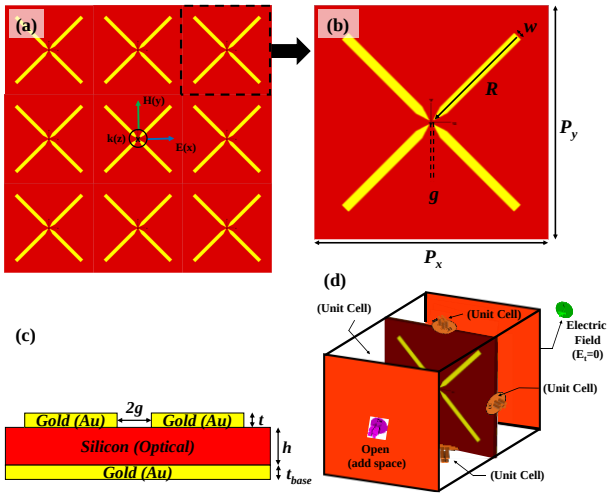

Figure 1. (a) Array of unit cell, (b) bird's eye view with design parameters, (c) lateral view, and (d) simulation medium

Silicon (optical) material, selected from the CST Microwave Studio program library and containing data in the 350-1500THz frequency band with a 10^{th}-order model with a dispersive epsilon value and a magnetic permeability of 1, was used as the substrate material

[30]. The design parameters are shown in Figure 1b, and the unit cell structure is depicted in lateral design views (Figure 1c). Furthermore, the design parameters in micrometers, resulting in the best absorption peak, are listed in Table 2. In order to conduct simulations, the suggested sensor creation is configured as metal-substrate-metal. The layered structure's upper surface has been covered with lossy Au, which has an electrical conductivity of σ = 4.561×107 S/m and a thickness of 0.1 μm, regardless of frequency. In the simulations, the bottom surface of the DBMA structure is covered with the same metal, which has a thickness of 0.4 μm. The finite Integration technique (FIT) was used for absorption performance simulations of the designed absorber. The unit cell receives illumination at normal incidence from a planar electromagnetic (EM) wave, where the x-axis represents the electric field (E-field) during the simulations. Perfectly matched layers are applied along the z-axis, and periodic boundary conditions are utilized in the x- and y-directions. (Figure 1d).

Table 2. Design parameters of the best performing TMA

g	h	P_x=P_y	R	t	t_{base}	w
1	4.5	100	52	0.1	0.4	4

Metamaterial surfaces absorb EM waves based on the theory of impedance matching. Part of the EM waves will be transmitted, and some will be reflected when they reach the metamaterial absorber surface. Hence, it follows that in order to guarantee optimal absorption, the transmission and reflection coefficients must be as low as feasible. For the best absorption results, the free space wave and the metal array's surface impedance must coincide. The following formula provides the metamaterial's absorption rate when there is a matching impedance between the air and the absorber [31]:

$$A(\omega) = 1 - R(\omega) - T(\omega) = 1 - |S_{11}(\omega)|^2 - |S_{21}(\omega)|^2 \quad (1)$$

A(ω) implies absorption, while *R(ω)* and *T(ω)* represent reflection and transmission, respectively. As known, $S_{11}(\omega)$ and $S_{21}(\omega)$ (as a function of frequency scattering parameters) obtained from the simulations yield R(ω) and T(ω), respectively. Simultaneous reflection and transmission coefficients can achieve the highest possible absorption rate. The thickness of the metallic surface on the substrate is such that T(ω) = 0, which means that the incoming wave cannot be transmitted. The rate of reflection is the primary factor influencing the metamaterial absorber's absorption property. Perfect absorption is attained in these circumstances, with a reflectance of about zero (R). Thus, the absorption formula, which is independent of the transmission parameter and solely reliant on reflection, can be stated as follows:

$$A(\omega) = 1 - R(\omega) = 1 - |S_{11}(\omega)|^2 \quad (2)$$

3. RESULTS AND DISCUSSION

3.1. Outcomes

Simulations using CST Microwave Studio (2023) were used to determine the absorption and assess the scattering characteristics (S_{11} and S_{21}). Figure 2 displays the results that were achieved. The normalized input impedance of the proposed TMA is obtained with the following formula:

$$Z = \pm\sqrt{\frac{(1+S_{11})^2 - S_{21}^2}{(1-S_{11})^2 - S_{21}^2}} \quad (3)$$

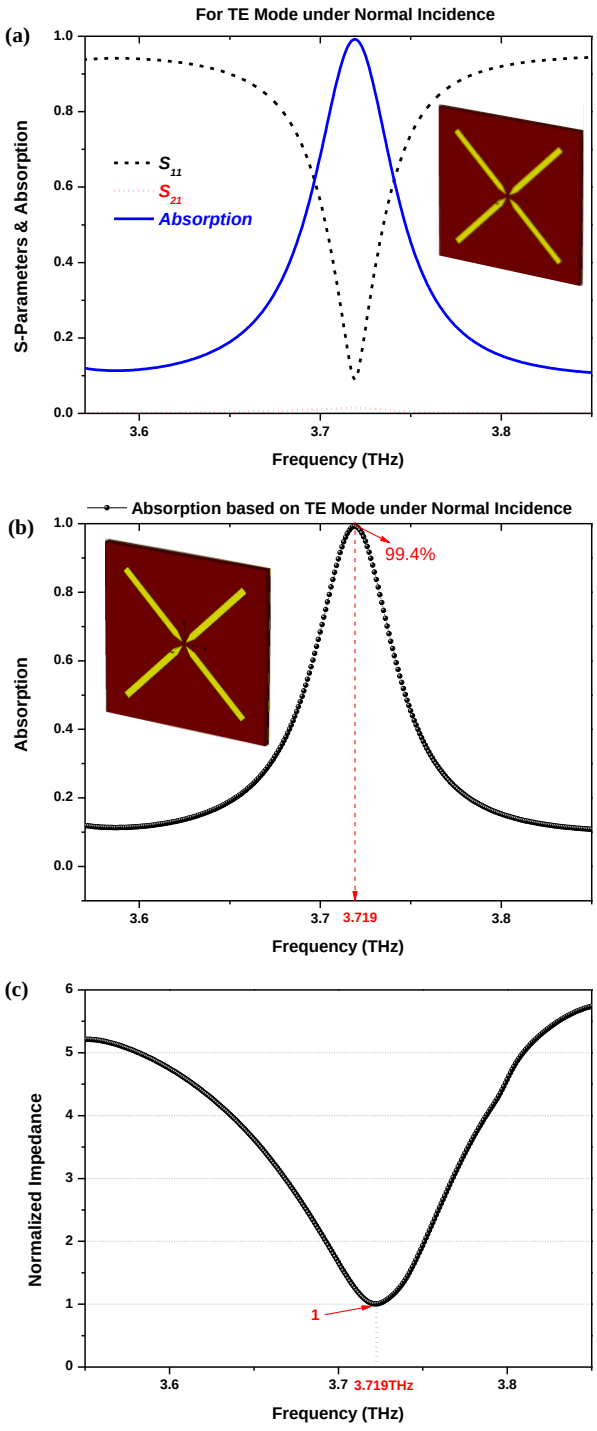

Figure 2. (a) S-parameters, (b) absorption spectra under normal oblique incidence angle, and (c) normalized impedance

A nearly perfect absorption at the operating frequency region can be achieved when the impedance matches between free space and a metamaterial absorber. It is valid if the normalized impedance of the free space (Z) is equal to 1 and equal to the normalized input impedance of the absorber. From Figure 2c, it is obviously seen that the condition of Z =Z_0=1 is obtained at the resonance frequency of 3.719 THz. The absorption is 99.4% when the surrounding medium's refractive index is the same as the free space's refractive index (η=1).

The absorption peak of 99.4% at 3.719 THz was obtained at the normal polarization angle (0 deg.) of incidence. To check the suitability of the proposed RIS for practical applications, it is plotted for various polarization angles from 0^0 to 90^0 in 15^0 increments, taking into account the normal incidence of the incident plane wave, as shown in Figure 3. All absorption resonance points have a high absorption rate of over 99.4%. In addition, there is no significant change in the absorption resonance points in the spectrum when the polarization angle rises significantly, showing that the presented absorber sensor is not sensitive to polarization and is suitable for practical applications [32]. It should be noted that this is an expected result due to the symmetrical structure of the geometry. In addition, it was observed that the absorber presented was sensitive depending on the oblique angle of incidence. Assuming that the angle of incidence is not vital for sensor applications, the absorption results based on the oblique incidence are not included here.

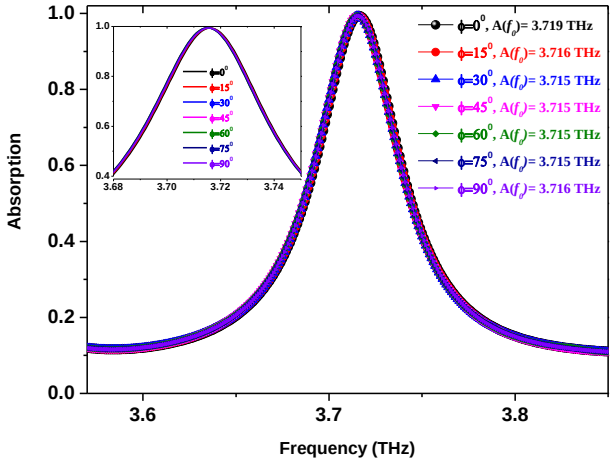

Figure 3. Absorption of the proposed sensor on different polarization angle

In sensing applications, the sensor is considered to be entirely surrounded by the encircling medium. When the medium thickness is much larger than the consistent length of the light wave arriving at the sensor, this thickness can be considered infinite [33]. The variation of absorption peaks according to the refractive index 'η' is given in Figure 4. There is a significant shift in the absorption peaks in the refractive index of the medium surrounding the sensor. The shift feature shows that the proposed absorber (PA) has acceptable high absorption peaks even with a slight change of 0.01 in the refractive index. Thus, it shows that the PA acts as an outstanding RIS. Additionally, the peak values of the absorption peaks according to the η changes are given in Table 3.

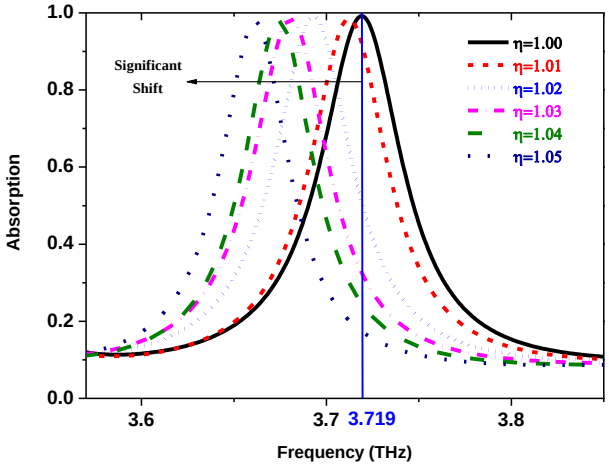

Figure 4. The absorption distributions of the proposed design based on changes in refractive index (η) of the encircling medium

Table 3. The absorption percentages based on the η, refractive index of the encircling medium

Refractive Index (η)	1.00	1.01	1.02	1.03	1.04	1.05
Absorption	99.20	98.60	99.00	98.77	98.00	97.75

By observing simulation results from Figure 2b, 99.2% absorption rate was reached by the structure at a narrow absorption peak located at 3.719 THz. As is well-known, the quality (Q-) factor can be determined from the equation of Q=*f* / FQHM [33], where FWHM is defined as the full width at half maximum and *f* is the resonance frequency of EM waves. The FWHM of the PA is found to be 0.06264 THz, while the resonance frequency of EM waves is 3.719 THz. According to the quality factor formula, the Q is obtained as 65.77.

In Figure 5, the resonance frequencies (f_0) as a function of the η are analyzed to understand the sensing performance according to the narrow absorption properties. The provided structure broadens the detecting region to obtain a noticeable sensing impact and reinforces the coupling of EM waves to produce a significant absorption effect. The obtained data from the resonant frequencies versus the refractive index is plotted with the linear fit of the data in Figure 5. The relationship between the resonant frequencies and the refractive index is determined by linear fitting as given in the equation of $f_0 = -1.2\eta + 4.922$.

Sensitivity is a critical factor to consider when assessing a sensor's ability to sense. As shown below, the ratio of the evolution in the resonance frequency (f_r) to the change of refractive index (η) can be used to determine sensitivity (*S*)[28]:

$$S = \frac{\Delta f_r}{\Delta \eta} \qquad (4)$$

where Δf_r and $\Delta \eta$ are the changes in the resonant frequency values and the refractive index, respectively. Thus, the sensitivity of the proposed RIS is approximately 1215 GHz/RIU.

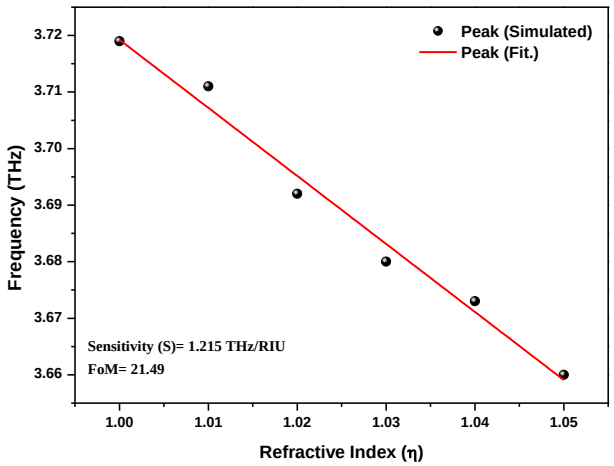

Figure 5. (a) The simulated resonant frequency distributions versus the refractive index (the red line shows the functions of the linear fit of the distributed data)

The ratio of sensitivity to FWHM of the absorber, called FoM, is another crucial parameter used to compare the detection performances of designed sensors. In our design, FoM was found to be 21.49. The high-quality factor, sensitivity as well as high FoM value make our design a high-quality RIS [33].

$$FoM = \frac{\mathrm{S}}{\mathrm{FWHM}} \qquad (5)$$

A parametrical investigation is provided in Figure 6 to justify the design parameters. From Figure 6a-c, the geometric parameters of the metasurface structure were analyzed at different values to obtain the best optimum absorption results.

The best optimal results are given above in Table 1. Finally, the proposed structure was designed in diagonal two-arm shapes to simulate absorption. As can be seen from Figure 6d, the best absorption results are possible when a symmetrical structure is obtained. To vividly understand the physical mechanism of the absorption generated by the PA, the electric and magnetic field distributions at the frequency (f_r=3.719 THz) corresponding to the absorption peak are calculated, respectively. While Figure 7a represents the electric field distribution on the upper surface (xoy-plane) of the presented absorber structure, Figure 7b shows the magnetic field distribution on the upper surface of the presented absorber. Figure 7c and d show the electric and magnetic field distributions in the xoz-plane, respectively. Figure 7a shows strong electric field distribution with regional charge accumulation in the absorber structure's arms. It can be concluded that the local charge accumulation in the arms leads to the fundamental dipole's excitation. It means that there exists a robust electrical resonance [28].

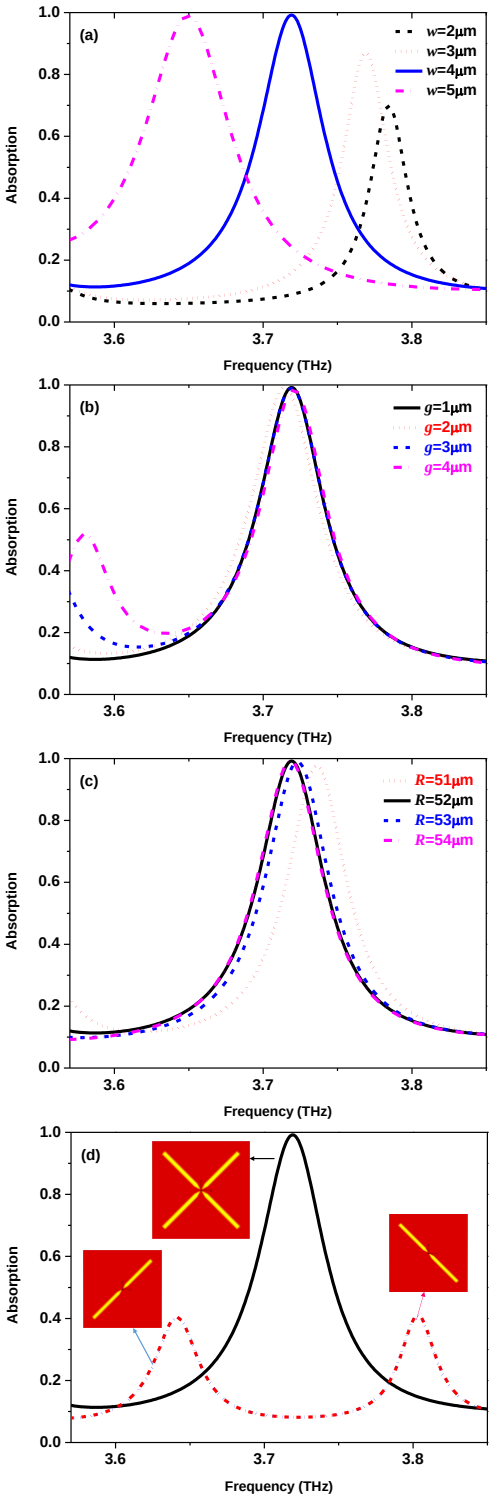

Figure 6. Parametric analysis based on (a) the width of each resonator, (b) the gap between resonators, (c) the length of each resonator, and (d) the number of resonators

From Figures 7b and d, the opposing charges formed between the metallic structure on the upper surface of the absorber structure and the layer on the lower surface (see Figures 3 and f) excite the magnetic dipole [34]. It is seen that a substantial magnetic field increase occurs in the center of the structure. Briefly, the occurrence of the fundamental absorption peak is facilitated by the simultaneous activation of electric and magnetic dipole resonances.

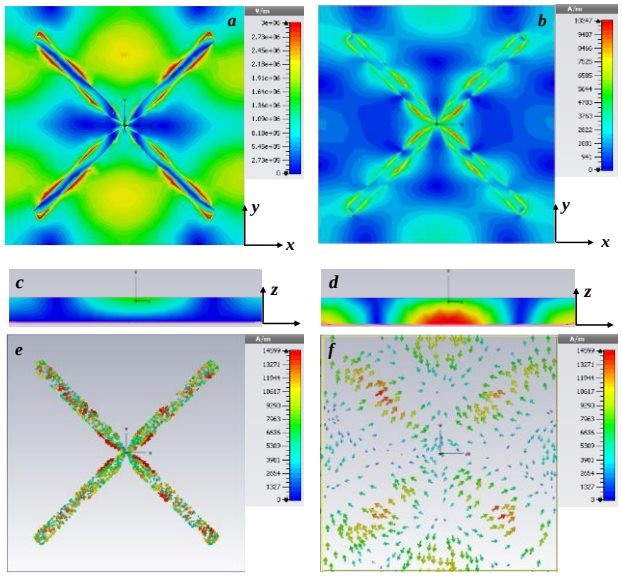

Figure 7. (a,b) Electric and magnetic field on xoy-plane, respectively, (c,d) electric and magnetic field on xoz-plane, respectively, (e) surface current distributions on the top surface, and (f) surface current distributions on the bottom surface

3.2. Equivalent Electrical Circuit Model

A method of quasi-static estimation to figure the equivalent circuit model of frequency selective surfaces (FSS) and metamaterial structures is known as an equivalent circuit approach. In this approach, the interaction of EM waves in infinite periodic arrays is assumed as an EM wave along a transmission line to present an array. This approach approximately transforms a metamaterial structure into an equivalent electrical circuit [35]. Using this technique, an equivalent circuit of the proposed TMA has been designed and simulated using the advanced design systems (ADS) [36]. A single port is assigned, considering zero transmission coefficient in the equivalent circuit because of the metal-backed design. Each arrow component of the PA has been considered an LC circuit, which has been parallely connected, assigned as L_1C_{1a} through L_4C_{4a}, with a series of capacitors, assigned as C_1 through C_4 (Fig. 8a,b). The capacitors C_{1a} through C_{4a} represent the capacitance formed between the arrow-shaped metal metasurface structures and the ground plane, while the capacitors C_1 through C_4 display the capacitance formed between the arrow components. The calculated input impedance from the equivalent circuit of the PA is revealed in Eq. (5), while the impedance of Z_4 is defined as $[j\omega L_4 + 1/j\omega C_{4a}]//(1/j\omega C_4)$. The input impedance value obtained using Equation 5 is obtained with Re(Z)=371.94 ohm and Imag(Z)=0.00175 values at 3.719THz resonance frequency. Based on this, it is understood that mismatching is achieved between the input impedance of the metasurface and the free-space impedance.

$$Z = \left[\left(\left(\left(\left(Z_4 + \frac{1}{j\omega C_3}\right)//Z_3\right) + \frac{1}{j\omega C_2}\right)/Z_2\right) + \frac{1}{j\omega C_1}\right]//Z_1 \quad (6)$$

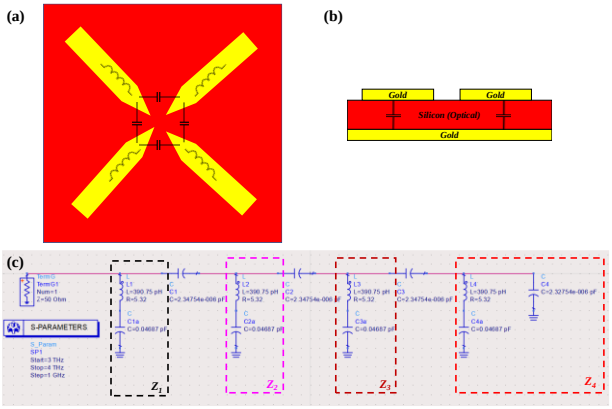

Figure 8. The equivalent electrical circuit diagram on (a) top surface view, (b) lateral view, and (c) the equivalent circuit of the PA with the values of the components in detail

For each identical component, the inductance and capacitance values formed between these structures and the ground plane are calculated as follows [37-39]:

$$L = 2\text{x}10^{-4} l[\ln(\frac{l}{w+t}) + 1.193 + 0.02235(\frac{w+t}{l})] \quad (7)$$

$$C = {}^{1}/_{(2\pi f_0)^2 L} \quad (8)$$

The *S*-parameter simulation of the equivalent circuit was chosen in the same range as the frequency range in the CST simulations. The results of the S_{11} parameter, as a function of frequency, are plotted in Fig. 8c using the electromagnetic simulation and the equivalent electrical circuit simulation. The results are in good agreement shown in Figure 9.

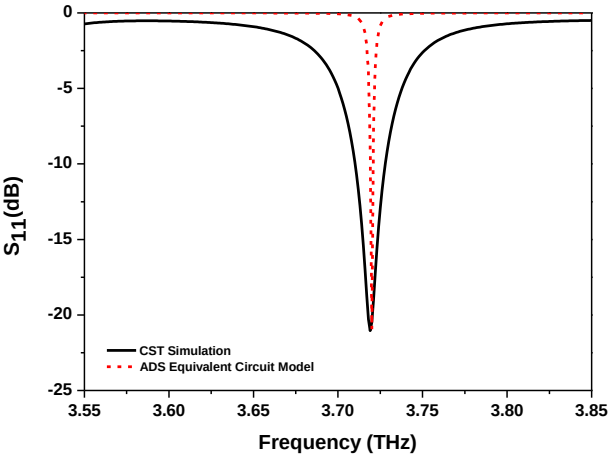

Figure 9. Comparison EM and equivalent electrical circuit simulation

4. CONCLUSION

This theoretical study presents a single-band THz metamaterial absorber in the THz regime that can be used as an outstanding refractive index sensor. An EM and equivalent electrical circuit simulations are compared regarding the S_{11} reflection coefficient (in dB-scale), resulting in a good agreement of findings by CST microwave studio and ADS. The proposed absorber is highly sensitive to changes in the surrounding medium's refractive index and has a polarization-independent property. From the analysis and the findings obtained, it is understood that this study demonstrates the theoretical feasibility and superior sensing performance. Theoretical findings show that the absorber-based sensor achieves a narrow peak absorption level of 99.20% at 3.719 THz. Geometric parameters can specifically be used to adjust the absorption. Further analysis reveals that electrical and magnetic resonances made the intended structure's efficient absorption possible. The absorber shows significant variations in the 3.719 THZ resonance frequency for different refractive indexes (0.01 steps size in the range of 1-1.05), and the sensitivity of the sensor is 1215GHz/RIU while the Q quality factor is 65.77 and the FoM is 21.49. Our work uses the designed terahertz metamaterial absorber as a refractive index sensor (RIS) to detect the change in the refractive index of different media.

Acknowledgement

This research has been supported by Bayburt University Scientific Research Projects Coordination Department, Project Number:2023/69002-04.

REFERENCES

[1] Saadeldin AS, Hameed MF, Elkaramany EM, Obayya SS. Highly sensitive terahertz metamaterial sensor. IEEE Sensors Journal. 2019 May 22;19(18):7993-9.

[2] Zhang Z, Ding H, Yan X, Liang L, Wei D, Wang M, Yang Q, Yao J. Sensitive detection of cancer cell apoptosis based on the non-bianisotropic metamaterials biosensors in terahertz frequency. Optical Materials Express. 2018 Mar 1;8(3):659-67.

[3] Palermo G, Lio GE, Esposito M, Ricciardi L, Manoccio M, Tasco V, Passaseo A, De Luca A, Strangi G. Biomolecular sensing at the interface between chiral metasurfaces and hyperbolic metamaterials. ACS applied materials & interfaces. 2020 Jun 18;12(27):30181-8.

[4] He X, Li S, Yang X, Shi S, Wu F, Jiang J. High-sensitive dual-band sensor based on microsize circular ring complementary terahertz metamaterial. Journal of Electromagnetic Waves and Applications. 2017 Jan 2;31(1):91-100.

[5] Geng Z, Zhang X, Fan Z, Lv X, Chen H. A route to terahertz metamaterial biosensor integrated with microfluidics for liver cancer biomarker testing in early stage. Scientific reports. 2017 Nov 27;7(1):16378.

[6] Li Y, Chen X, Hu F, Li D, Teng H, Rong Q, Zhang W, Han J, Liang H. Four resonators based high sensitive terahertz metamaterial biosensor used for measuring concentration of protein. Journal of Physics D: Applied Physics. 2019 Jan 2;52(9):095105.

[7] Park JW, Vu DL, Zheng HY, Rhee JY, Kim KW, Lee YP. THz-metamaterial absorbers. Advances in Natural Sciences: Nanoscience and Nanotechnology. 2013 Jan 18;4(1):015001.

[8] Shrekenhamer D, Montoya J, Krishna S, Padilla WJ. Four-color Metamaterial absorber THz spatial light modulator. Advanced Optical Materials. 2013 Dec;1(12):905-9.

[9] Zhu J, Ma Z, Sun W, Ding F, He Q, Zhou L, Ma Y. Ultra-broadband terahertz metamaterial absorber. Applied Physics Letters. 2014 Jul 14;105(2).

[10] Grant J, Escorcia-Carranza I, Li C, McCrindle IJ, Gough J, Cumming DR. A monolithic resonant terahertz sensor element comprising a metamaterial absorber and micro-bolometer. Laser & Photonics Reviews. 2013 Nov;7(6):1043-8.

[11] Carranza IE, Grant J, Gough J, Cumming DR. Metamaterial-based terahertz imaging. IEEE Transactions on Terahertz Science and Technology. 2015 Aug 21;5(6):892-901.

[12] Duan G, Schalch J, Zhao X, Li A, Chen C, Averitt RD, Zhang X. A survey of theoretical models for terahertz electromagnetic metamaterial absorbers. Sensors and Actuators A: Physical. 2019 Mar 1;287:21-8.

[13] Anik MH, Mahmud S, Mahmood KS, Isti MI, Talukder H, Biswas SK. Numerical investigation of a gear-shaped triple-band perfect terahertz metamaterial absorber as biochemical sensor. IEEE Sensors Journal. 2022 Aug 8;22(18):17819-29.

[14] Cheng D, He X, Huang X, Zhang B, Liu G, Shu G, Fang C, Wang J, Luo Y. Terahertz biosensing metamaterial absorber for virus detection based on spoof surface plasmon polaritons. International Journal of RF and Microwave Computer-Aided Engineering. 2018 Sep;28(7):e21448.

[15] Shen S, Liu X, Shen Y, Qu J, Pickwell-MacPherson E, Wei X, Sun Y. Recent advances in the development of materials for terahertz metamaterial sensing. Advanced Optical Materials. 2022 Jan;10(1):2101008.

[16] Banerjee S, Dutta P, Basu S, Mishra SK, Appasani B, Nanda S, Abdulkarim YI, Muhammadsharif FF, Dong J, Jha AV, Bizon N. A New Design of a Terahertz Metamaterial Absorber for Gas Sensing Applications. Symmetry. 2022 Dec 22;15(1):24.

[17] Mehrotra P. Biosensors and their applications–A review. Journal of oral biology and craniofacial research. 2016 May 1;6(2):153-9.

[18] Liu J, Fan L, Su J, Yang S, Luo H, Shen X, Ding F. Study on a terahertz biosensor based on graphene-metamaterial. Spectrochimica Acta Part A: Molecular and Biomolecular Spectroscopy. 2022 Nov 5;280:121527.

[19] Guo W, Zhai L, El-Bahy ZM, Lu Z, Li L, Elnaggar AY, Ibrahim MM, Cao H, Lin J, Wang B. Terahertz metamaterial biosensor based on open

square ring. Advanced Composites and Hybrid Materials. 2023 Jun;6(3):92.
[20] Jianjun L, Lanlan F. Development of a tunable terahertz absorber based on temperature control. Microwave and Optical Technology Letters. 2020 Apr;62(4):1681-5.
[21] Zou H, Cheng Y. Design of a six-band terahertz metamaterial absorber for temperature sensing application. Optical Materials. 2019 Feb 1;88:674-9.
[22] Banerjee S, Nath U, Jha AV, Pahadsingh S, Appasani B, Bizon N, Srinivasulu A. A terahertz metamaterial absorber based refractive index sensor with high quality factor. In2021 13th International Conference on Electronics, Computers and Artificial Intelligence (ECAI) 2021 Jul 1 (pp. 1-4). IEEE.
[23] Bai J, Shen W, Wang S, Ge M, Chen T, Shen P, Chang S. An ultra-thin multiband terahertz metamaterial absorber and sensing applications. Optical and Quantum Electronics. 2021 Sep;53(9):506.
[24] Yahiaoui R, Tan S, Cong L, Singh R, Yan F, Zhang W. Multispectral terahertz sensing with highly flexible ultrathin metamaterial absorber. Journal of Applied Physics. 2015 Aug 28;118(8).
[25] Singh R, Cao W, Al-Naib I, Cong L, Withayachumnankul W, Zhang W. Ultrasensitive terahertz sensing with high-Q Fano resonances in metasurfaces. Applied Physics Letters. 2014 Oct 27;105(17).
[26] Li Y, Chen X, Hu F, Li D, Teng H, Rong Q, Zhang W, Han J, Liang H. Four resonators based high sensitive terahertz metamaterial biosensor used for measuring concentration of protein. Journal of Physics D: Applied Physics. 2019 Jan 2;52(9):095105.
[27] Shen F, Qin J, Han Z. Planar antenna array as a highly sensitive terahertz sensor. Applied optics. 2019 Jan 20;58(3):540-4.
[28] Yu J, Lang T, Chen H. All-metal terahertz metamaterial absorber and refractive index sensing performance. Photonics. 2021 May 14;8(5): 164).
[29] Wang BX, He Y, Lou P, Xing W. Design of a dual-band terahertz metamaterial absorber using two identical square patches for sensing application. Nanoscale Advances. 2020;2(2):763-9.
[30] Palik ED, editor. Handbook of optical constants of solids. Academic press; 1998.
[31] Kong X, Jiang S, Kong L, Wang Q, Hu H, Zhang X, Zhao X. Transparent metamaterial absorber with broadband radar cross-section (RCS) reduction for solar arrays. IET Microwaves, Antennas & Propagation. 2020 Oct;14(13):1580-6.
[32] Shen X, Cui TJ, Zhao J, Ma HF, Jiang WX, Li H. Polarization-independent wide-angle triple-band metamaterial absorber. Optics express. 2011 May 9;19(10):9401-7.
[33] Banerjee S, Nath U, Dutta P, Jha AV, Appasani B, Bizon N. A theoretical terahertz metamaterial absorber structure with a high quality factor using two circular ring resonators for biomedical sensing. Inventions. 2021 Nov 2;6(4):78.
[34] Guddala S, Kumar R, Ramakrishna SA. Thermally induced nonlinear optical absorption in metamaterial perfect absorbers. Applied Physics Letters. 2015 Mar 16;106(11).
[35] Zhao M, Xu J, Zhao J. Design and analysis of dual-band FSS based on equivalent circuit. International Journal of RF and Microwave Computer-Aided Engineering. 2022 Dec;32(12):e23405.
[36] Keysight Headquarters [Internet], Available from: https://www.keysight.com/us/en/products/software/pathwave-design-software/pathwave-advanced-design-system.html
[37] Islam MS, Samsuzzaman M, Beng GK, Misran N, Amin N, Islam MT. A gap coupled hexagonal split ring resonator based metamaterial for S-band and X-band microwave applications. IEEE Access. 2020 Apr 6;8:68239-53.
[38] Singh AK, Abegaonkar MP, Koul SK. Dual-and triple-band polarization insensitive ultrathin conformal metamaterial absorbers with wide angular stability. IEEE Transactions on Electromagnetic Compatibility. 2018 Jun 20;61(3):878-86.
[39] Hakim ML, Alam T, Islam MT, Alsaif H, Soliman MS. Polarization-independent fractal square splits ring resonator (FSSRR) multiband metamaterial absorber/artificial magnetic conductor/sensor for Ku/K/Ka/5G (mm-Wave) band applications. Measurement. 2023 Mar 31;210:112545.